Dynamic measurement of forward scattering

Appel-Hansen, Jørgen; Rusch, W.

Published in:
I E E E Transactions on Antennas and Propagation

Publication date:
1975

Document Version
Publisher's PDF, also known as Version of record

[4] D. S. Jones, *The Theory of Electromagnetism*. New York: Pergamon, 1964, pp. 329–332.
[5] J. Strong, *Concepts of Classical Optics*. San Francisco, Calif.: Freeman, 1958, pp. 128–133.
[6] T. Morita and S. B. Cohn, "Microwave lens matching by simulated quarter-wave transformers," *IRE Trans. Antennas Propagat.*, vol. AP-4, pp. 33–39, Jan. 1956.
[7] R. E. Collin, *Field Theory of Guided Waves*. New York: McGraw-Hill, 1960, pp. 97–102.
[8] A. E. Philippe, "Reflection and transmission of radio waves at a dielectric slab with variable permittivity," *IEEE Trans. Antennas Propagat.* (Commun.), vol. AP-21, pp. 234–236, Mar. 1973.

Dynamic Measurement of Forward Scattering

J. APPEL-HANSEN AND W. V. T. RUSCH

Abstract—**A dynamic method for the measurement of forward scattering in a radio anechoic chamber is described. The quantity determined is the induced-field-ratio (IFR) of conducting cylinders. The determination of the IFR is highly sensitive to 1) multiple scattering between the cylinder and the obpring antenna and 2) extraneous scattering from the lining of the anechoic chamber. In order to eliminate the influence of multiple scattering, the measurements are made dynamically, i.e., the cylinders are mounted on a moving cart. The consequences of this movement are analyzed. Experimental data are presented in terms of the dynamic measurements. The influence of extraneous scattering is evaluated and an indication of a method for reducing errors due to extraneous scattering is given.**

I. Introduction

Free space forward scattering measurements from a generalized test object present many unique problems which are not found in other types of scattering measurements. A recently conducted program for the measurement of forward scattering by struts for a microwave reflector antenna [1] demanded the development of an extremely sensitive method to measure forward scattering, inasmuch as the scattered field was relatively weak. Although in this case the test objects were long thin metallic cylinders of square and circular cross sections, the technique is applicable to any kind of a test object.

The induced-field-ratio (IFR) is defined as the (complex) ratio of the forward-scattered field from a scatterer immersed in an incident plane wave to the field radiated by a planar aperture of the same cross section illuminated by the same wave. It is thus directly proportional to the forward scattered field, and provides a standard, normalized complex parameter useful in the characterization of forward scattering. In the "optical" limit, the IFR of a test object approaches unity in magnitude and 180° in phase. In its customary two-dimensional sense, the IFR of an infinite conducting cylinder of arbitrary cross section immersed in a normally incident plane wave polarized parallel to the axis of the cylinder (*E*-wave case) is

$$\mathrm{IFR}_E = -\frac{Z_0}{2WE_0}\oint_S J_{Sz}\exp\left[jk\rho'\cos\left(\phi'-\frac{\pi}{2}\right)\right]dS' \quad (1)$$

where ρ',ϕ' are integration variables, dS' is the differential path length around the periphery, $Z_0 \simeq 120\pi$, E_0 is the intensity of the incident field, W is the maximum width of the cylinder transverse to the wave normal and J_{Sz} is the induced, axially flowing, surface current density on the cylinder [1]. Similarly, for the *H*-wave case

$$\mathrm{IFR}_H = -\frac{1}{2WH_0}\oint_S J_{St}(\boldsymbol{a}_k\cdot\boldsymbol{n})\exp\left[jk\rho'\cos\left(\phi'-\frac{\pi}{2}\right)\right]dS' \quad (2)$$

where H_0 is the intensity of the incident magnetic field, $\boldsymbol{a}_k$ is the wave-normal direction, $\boldsymbol{n}$ is the surface normal, and J_{St} is the induced, circumferential flowing, surface current density on the cylinder.

The measurement of two-dimensional scattering parameters of metallic cylinders of arbitrary cross section is best carried out for *E*-polarization in a parallel-plate waveguide. An alternative scheme for both *E*- and *H*-polarization is the use of a three-dimensional scattering range using relatively narrow-beam horns which do not significantly illuminate the ends of long thin scatterers used to represent the infinite structure [2]. This three-dimensional technique has been used by the authors to determine the IFR of square and circular cylinders.

To provide useful results it was necessary to place confidence in the measurements to within 0.05 dB of attenuation and 0.05° of phase. Thus, it became necessary to analyze the effects of 1) multiple scattering between the test object and the receiving horn and 2) extraneous scattering, i.e., reflections from the walls, floor, and ceiling of the radio anechoic chamber. The following sections will discuss the measurement technique, whereby the test object is moved continuously in a central region between the two horns. It will be shown that this dynamic method eliminates the influence of multiple scattering and thereby increases measurement accuracy. Furthermore, an analysis of the effect of extraneous scattering will be included as a means of indicating, under worst-case conditions, the uncertainty of the measured IFR values. In addition to this, it will be indicated how the influence of extraneous scattering may be reduced if necessary.

To the knowledge of the authors the presented use of the moving-target technique for measurement of forward scattering is new. However, it should be mentioned that different other uses of the moving-target techniques in both backscattering and bistatic scattering measurements have been used in the past [3]–[8].

II. Analytical Formulation

When the cylindrical test object is located approximately midway between coaxial transmitting and receiving horns (see Fig. 1) it may be shown that, to the extent that the cylinder is long in terms of wavelength and that end effects may be neglected [1],

$$\mathrm{IFR} = \frac{E_s}{E_i}\frac{e^{-j\pi/4}}{W}\sqrt{\frac{\lambda\eta_0\eta_0'}{\eta_0+\eta_0'}} \quad (3)$$

where E_i is the direct field of the transmitting horn incident on the receiving horn, E_s is the field of the induced currents on the cylinder, η_0 and η_0' are the distances from the transmitting horn to cylinder axis and from receiving horn to cylinder axis, respectively. This expression is valid for both polarizations. As will be shown in Section V, when extraneous signals may be neglected, the field ratio in (3) may be expressed in terms of the measured attenuation $\Delta\alpha$ and measured phase shift $\Delta\phi$ due to the presence of the cylinder. Thus (3) reduces to

$$\mathrm{IFR} \simeq (e^{-\Delta\alpha}e^{-j\Delta\phi}-1)\frac{e^{-j\pi/4}}{W}\sqrt{\frac{\lambda\eta_0\eta_0'}{\eta_0+\eta_0'}}. \quad (4)$$

Manuscript received January 27, 1975; revised May 31, 1975.
J. Appel-Hansen is with the Electromagnetics Institute, Radio Anechoic Chamber, Technical University of Denmark, Lyngby, Denmark.
W. V. T. Rusch is with the Electromagnetics Institute, Technical University of Denmark, Lyngby, Denmark, on leave from the Department of Electrical Engineering, University of Southern California, Los Angeles, Calif. 90007.

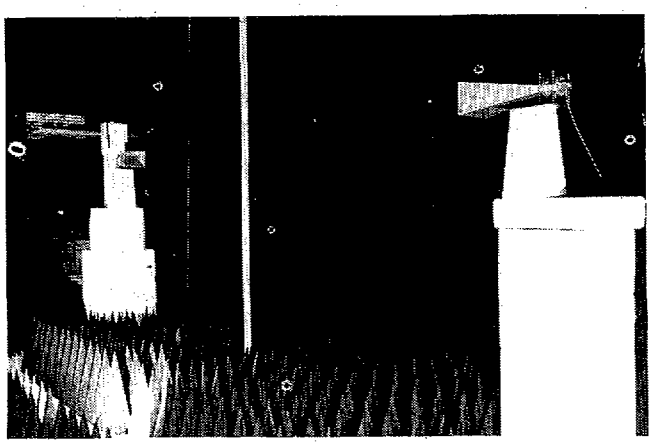

Fig. 1. Experimental setup in radio anechoic chamber.

Since $\Delta\alpha$ may be only a very small fraction of a decibel and $\Delta\phi$ only a few degrees, the bracketed expression in (4) is subtracting two very nearly equal quantities. Therefore the resulting IFR's are highly susceptible to measurement errors. The remainder of this paper deals with a method by which the effects of these measurement errors may be reduced.

III. Experimental Setup

The experiments are carried out in a radio anechoic chamber as shown in Fig. 1. The test object is mounted in a support placed below the base level of the floor absorbers. The support is placed on a cart which rolls on rails as shown in Fig. 2. It is seen that a frequency stabilized signal is guided to a transmission test unit which is connected to transmitting and receiving horns. Furthermore, the transmission test unit is connected to a network analyzer. By means of this analyzer, amplitude and phase changes in the transmission link between the two horns can be observed on the meter. Moreover, the analyzer delivers a dc signal proportional to the amplitude or phase indication depending on the mode of operation selected. By means of a dc chopper-amplifier this signal is introduced into a recorder. The chart of this recorder is coupled to the movements of the rolling cart by means of a synchro.

In principle the measurements are carried out in the following manner. Without the test object in its support, the rolling cart is moved about two wavelengths and the levels of amplitude and phase are recorded. Then the test object is inserted, the rolling cart is moved again, and the new levels of amplitude and phase are recorded. As illustrated in Fig. 2, the amplitude change $\Delta\alpha$ and phase change $\Delta\phi$ caused by the test object can be found from the recordings. In order to find $\Delta\alpha$ and $\Delta\phi$, the chart of the recorder is calibrated using phase and gain verniers of the network analyzer. The component of the measured signal and the reduction of data are described in the next sections.

IV. The Measured Signal

In Fig. 3 is shown the measured signal without and with the test object inserted between the transmitting and receiving horns. The measured signal E_m^i without the test object consists of the incident field E_i from the transmitting horn to the receiving horn and the extraneous scattered field E_r^i, i.e., the reflections from the walls, floor, and ceiling of the anechoic chamber. The incident field E_i varies in the usual manner with the distance between the two horns. Since E_r^i consists of reflections from the different

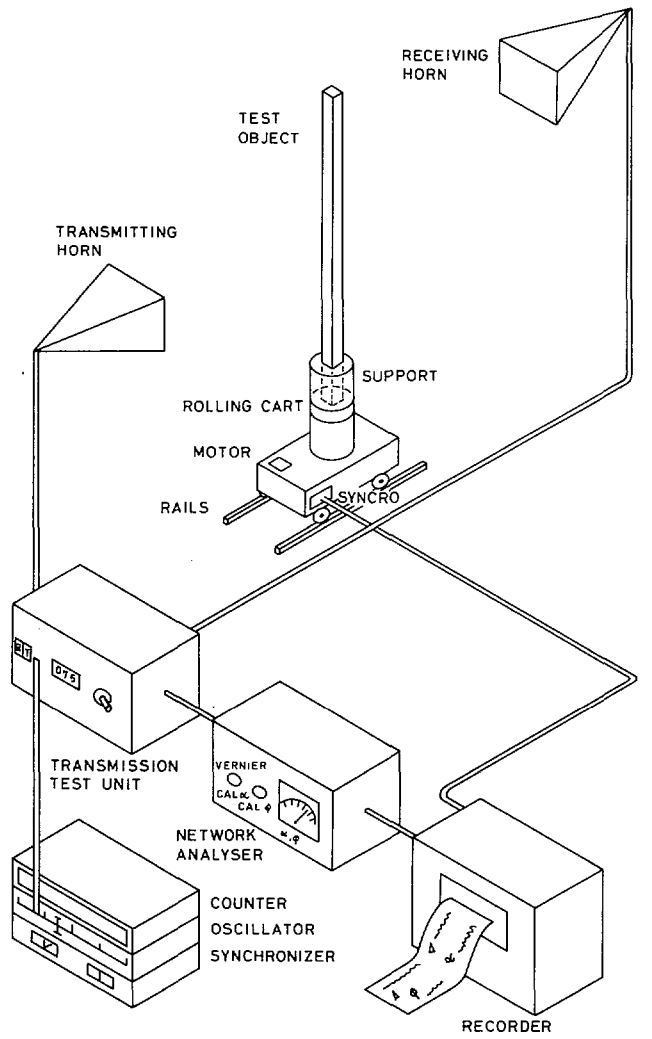

Fig. 2. Experimental setup.

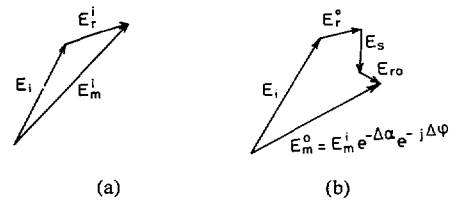

Fig. 3. Measured signal without and with test object inserted. (a) Without test object. (b) With test object.

parts of the chamber, E_r^i varies in a complicated manner with the position of the receiving horn.

As described in the previous section, the amplitude and phase changes of the measured signal are recorded when the test object is inserted. It appears in Fig. 3(b) that under this condition, the measured signal $E_m^0 = E_m^i e^{-\Delta\alpha} e^{-j\Delta\phi}$ consists of the following four components.

1) The incident field E_i described above.

2) The extraneous scattered field E_r^0 from the walls, floor, and ceiling of the anechoic chamber. The difference between E_r^0 and E_r^i is due to the change in illumination of the lining of the anechoic chamber caused by the insertion of the test object. However, usually there will not be a significant difference between E_r^0 and E_r^i.

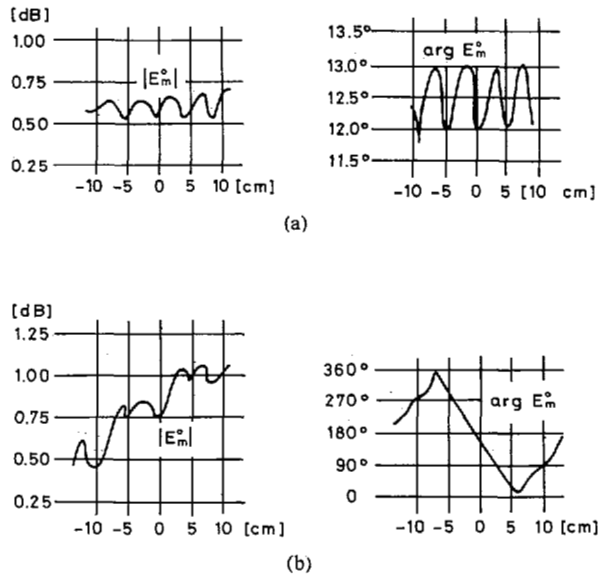

Fig. 4. Examples of recorded curves. (a) Movement of test object. (b) Movement of receiving horn.

3) The field E_s scattered from the test object.

4) The component E_{r0} due to multiple scattering between the horns and the test object.

We have not made a detailed and general analysis of the influence of all the possible multiple scattering components between the two horns and the test object. However, as described below, we have observed that by moving the test object, the received signal varies similarly to a standing wave curve. This variation is attributed to multiple scattering. For example, multiple scattering between the two horns may cause a standing wave and thus the illumination of the test object may vary with the position of the test object. In fact, it seems likely that a major contribution to E_{r0} is a reflection between the receiving horn (including its support), the test object, and back to the receiving horn. This conclusion has been reached by analyzing variations in the recorded values of $|E_m^0|$ when the following movements were carried out:

1) movement of the test object;
2) movement of the receiving horn with and without the test object inserted.

Furthermore, for the purpose of enhancing multiple scattering in order to determine its source, metal plates have been mounted temporarily near the horns during some of the movements. Only in the cases where the test object was inserted and a metal plate was placed near the receiving horn, the variations in $|E_m^0|$ were increased (compared to variations without a metal plate). In addition to this, it should be mentioned that by inserting an isolator in the transmitting horn line, it was found that reflections between the cylinder and transmitting horn have no detectable influence on our results in the actual setup, i.e., there is a high degree of isolation between the transmitting channel and the receiving channel. It should be emphasized that the influence of multiple scattering may vary with the type of experimental setup. A first attempt to a more detailed analysis would be to probe the field between the two horns without the test object inserted.

In order to describe the nature of the recorded variations in $|E_m^0|$ and the manner in which the influence of E_{r0} was eliminated, it is convenient to refer to Fig. 3(b). When the test object is moved a short distance, E_i does not change, and E_s only has small amplitude changes. These changes and the variations in E_r^0 can be neglected. Thus, there will only be a variation in $|E_m^0|$ due to changes in E_{r0}, i.e., E_{r0} goes in- and out-of-phase with the sum of the remaining components. As shown in Fig. 4(a) the result is that a curve similar to a standing wave curve is recorded when the test object is moved. In the case where the receiving horn is moved when the test object is inserted, all four components of E_m^0 vary in amplitude and phase. As shown in Fig. 4(b), the curve recorded for $|E_m^0|$ in this case has a sloping character due to the decrease in $|E_i|$ with increasing distance between the two horns.

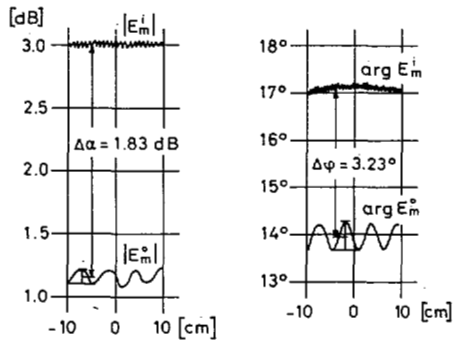

Fig. 5. Reduction of actually measured curves.

Movement of the test object furthermore causes the oscillatory phase characteristic seen in Fig. 4(a) due to the interference of E_{r0} (small) with the constant sum of the remaining components (large). On the other hand, movement of the receiving horn introduces approximately 360° of linear phase change for every wavelength of movement.

Thus, due to the regular character of the recorded curves when the test object is moved, the influence of E_{r0} can be eliminated, simply by averaging the amplitude and phase curves.

V. Reduction of Recorded Data

In order to determine the IFR of the test object, the amplitude and phase of E_m^i and E_m^0 are recorded during a movement of about two wavelengths. An example of recorded data is shown in Fig. 5. Without the test object inserted, of course, a movement of the cart is not required. However, instead of a point, it is convenient to have a line indicating the level of $|E_m^i|$ and arg E_m^i. Furthermore, the levels of $|E_m^i|$ and arg E_m^i are recorded just before and after the recordings of the curves for $|E_m^0|$ and arg E_m^0. This is not shown in Fig. 5, but is done in order to check the stability of the experimental setup for each determination of $\Delta\alpha$ and $\Delta\phi$.

Without the test objects mounted in its support (see Fig. 3)

$$E_m^i = E_i + E_r^i \tag{5}$$

and with the test object inserted

$$E_m^0 = E_i + E_r^0 + E_s + E_{r0}. \tag{6}$$

By averaging the curves for $|E_m^0|$ and arg E_m^0 as indicated in Fig. 5, the influence of the multiple scattering component E_{r0} is essentially eliminated. Thus, setting $E_{r0} = 0$ and introducing $\Delta\alpha$ and $\Delta\phi$ as shown in Fig. 5, we find from Fig. 3, (5) and (6),

$$(E_i + E_r^i)e^{-\Delta\alpha}e^{-j\Delta\phi} = E_i + E_r^0 + E_s \tag{7}$$

or

$$\frac{E_s}{E_i} = e^{-\Delta\alpha}e^{-j\Delta\phi} - 1 + \frac{E_r^i e^{-\Delta\alpha}e^{-j\Delta\phi} - E_r^0}{E_i}. \tag{8}$$

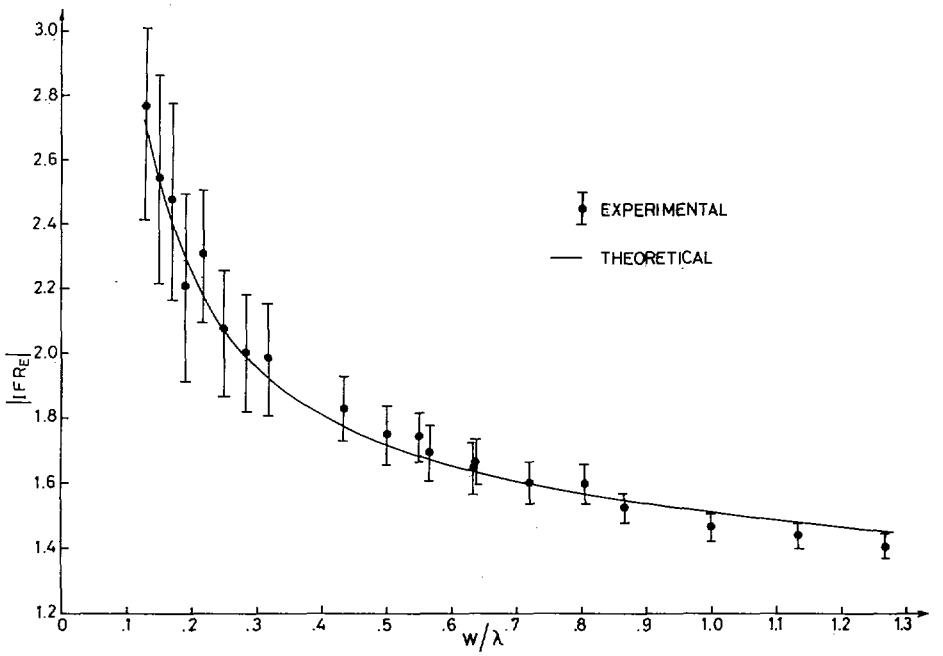

Fig. 6. IFR_E magnitude for square cylinder.

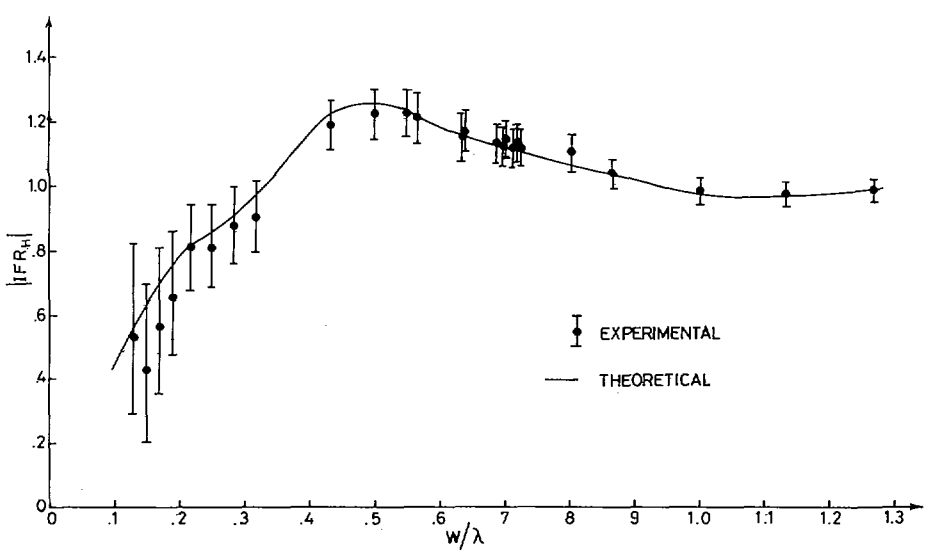

Fig. 7. IFR_H magnitude for square cylinder.

TABLE I
E-POLARIZATION

Cylinder / Method	Square Cylinder		Circular Cylinder	
	peak Δ	average |Δ|	peak Δ	average |Δ|
Stationary	23.5%	3.3%	9.3%	2.8%
Dynamic	5.5%	2.3%	6.5%	2.6%

TABLE II
H-POLARIZATION

Cylinder / Method	Square Cylinder		Circular Cylinder	
	peak Δ	average |Δ|	peak Δ	average |Δ|
Stationary	9.4%	3.3%	11.4%	3.8%
Dynamic	7.5%	1.9%	12.6%	3.2%

Since E_r^0 is of the same magnitude as E_r^i and $\Delta\alpha$ may be close to 0 dB, a rough estimation of the influence of extraneous reflections in the worst-case can be made from

$$\frac{E_s}{E_i} = e^{-\Delta\alpha}e^{-j\Delta\phi} - 1 + 2\frac{|E_r^i|}{|E_i|}e^{j\beta} \tag{9}$$

by properly choosing the introduced phase β. In the present measurements it was found by moving the receiving horn that $2(|E_r^i|/|E_i|) \simeq 0.006$. This means that, in particular for the larger cylinders, the extraneous reflections can be neglected, and it is found that

$$\frac{E_s}{E_i} \simeq e^{-\Delta\alpha}e^{-j\Delta\phi} - 1. \tag{10}$$

For all cylinders, we decided to use (4) and (10) for the determination of IFR and to use (4) and (9) to evaluate the influence of extraneous reflections and experimental uncertainties in $\Delta\alpha$ and $\Delta\phi$, see next section.

At this point it should be mentioned that in cases where $2(|E_r^i|/|E_i|)$ is known for the test range, (9) can be used to determine the smallest measurable |IFR| for given measurement accuracy. However, it should also be noted that the influence of extraneous scattering can be reduced by carrying out dynamic measurements for several fixed positions of the receiving horn and averaging the results. Of course, this will be a rather lengthy process and our resources did not extend so far.

VI. Results

Figs. 6 and 7 are plots of the measured and theoretical IFR magnitudes for a square cylinder for both *E*- and *H*-polarization. The error flags were determined from (9) by using $2(|E_r^i|/|E_i|) = 0.006$ and estimated experimental uncertainties of 0.05 dB and 0.05° in $\Delta\alpha$ and $\Delta\phi$, respectively. It is seen that the error flags, with one or two exceptions, overlap the theoretical curves.

Comparison of these dynamic results with comparable measurements made for a fixed test object yields the results shown in Tables I and II. The peak deviation between measurement and theory, and the average of the magnitude (regardless of sign) deviation are tabulated. The average deviation are generally slightly less in the dynamic measurements. However, the peak deviations are significantly less (except for the *H*-polarization, circular cylinder). This indicates that a measurement with a fixed test object will occasionally produce data strongly involving multiple scattering signals, i.e., a test point lying in one of the hills or valleys shown in the curves of Figs. 4 and 5.

VII. Conclusions

The dynamic method for the measurement of forward scattering in a radio anechoic chamber provides a method to discriminate against undesired multiple scattering. This technique is applicable to highly sensitive measurements requiring measured fields accurate to within 0.05 dB and 0.05° of phase. Agreement between experiment and theory will generally average 2–3 percent, with rare peak deviations as large as 10–12 percent. The influence of extraneous scattering is evaluated and a method to reduce the influence of the extraneous scattering is suggested.

Acknowledgment

The authors with to thank P. Laugesen and N. O. Nielsen who performed most of the measurement work and mechanical arrangements.

References

[1] W. V. T. Rusch, J. Appel-Hansen, C. A. Klein, and R. Mittra, "Forward scattering from square cylinders in the resonance region with application to aperture blockage," to be published.
[2] M. G. Andreasen and A. F. Kay, "Scattering from a metallic cylinder of arbitrary cross-section," TRG FR-220-2, Nov. 9, 1962.
[3] R. E. Hiatt, E. F. Knott, and T. B. A. Senior, "A study of VHF absorbers and anechoic rooms," Radiation Laboratory, Univ. of Michigan, Ann Arbor, Rep. 5391-1-F, Feb. 1963.
[4] J. Wilcox Philips, "Very small radar cross-section measurements at UHF," in *Radar Reflectivity Measurements Symp.*, RADC-TDR-64-25, Apr. 1964.
[5] O. P. McDuff, H. Mott, and C. S. Durrett, Jr., "Back-scattering measurements of a slowly moving target," *IEEE Trans. Microwave Theory Tech.*, vol. MTT-12, pp. 541–546, Sept. 1964.
[6] C. I. Beard, T. H. Kays, and V. Twersky, "Scattered intensities for random distributions—microwave data and optical applications," *Appl. Opt.*, vol. 4, p. 1299, 1965.
[7] A. C. Lind, R. T. Wang, and J. M. Greenburg, "Microwave scattering by nonspherical particles," *Appl. Opt.*, vol. 4, p. 1555, 1965.
[8] J. Appel-Hansen, "A Van Atta reflector consisting of half-wave dipoles," *IEEE Trans. Antennas Propagat.*, vol. AP-14, pp. 694–700, Nov. 1966.

Phase and Amplitude Scintillations at 9.6 GHz on an Elevated Path

M. C. THOMPSON, HARRIS B. JANES, MEMBER, IEEE, LOCKETT E. WOOD, AND DEAN SMITH

***Abstract*—Deep fading, e.g., > 40 dB, was observed at 9.6 GHz on a 150 km path with terminals at 3025 and 3300 m elevations and with no significant illumination of the earth's surface. Fades at two antennas**

Manuscript received November 10, 1974; revised June 9, 1975. This work was supported by the National Aeronautics and Space Administration under NASA Contract Order L-31028.

The authors are with the Institute for Telecommunications Sciences, Office of Telecommunications, U.S. Department of Commerce, Boulder, Colo. 80302.